Large Eddy Simulation of HAWT and VAWT performances in the vicinity of a building

Large Eddy Simulation of HAWT and VAWT performances in the vicinity of a building

P. Tene Hedje[1], S. Zeoli[1], U. Vigny[1,2], F. Houtin-Mongrolle[2], P. Benard[2] and L. Bricteux[1]

[1] Université de Mons (UMONS), Faculty of engineering, 20 Place du Parc,7000 Mons, Belgium.
[2] CORIA, CNRS UMR6614, Normandie Université, INSA and University of Rouen, 76801 Saint-Etienne-du-Rouvray, France.

E-mail: patrick.tenehedje@umons.ac.be

Abstract. This work compares the performances of a Horizontal Axis Wind Turbine (HAWT) and a Vertical Axis Wind Turbine (VAWT) using Wall modeled Large Eddy Simulation (WMLES) coupled with an actuator line method. The wind turbines are located in the vicinity of a real size industrial building. Both wind turbines are sized to produce the same power at their respective optimum Tip Speed Ratio for a same incident wind speed. Two relevant incident wind directions (SW and SSW) are investigated, the influence of the building on the performance of the two wind turbines is also analysed. The results obtained show that the HAWT has a better overall performance compared to the VAWT. Overspeeds are observed for both directions analysed, due to the presence of the building which locally increases the flow velocity. However, these overspeeds remain low due to the low height of the building. The change of wind direction only slightly impacts the HAWT production, while the VAWT production remains insensitive. However, the presence of the building improves the global production of both wind turbines. Qualitatively, this change of wind direction induces a deviation in the wake of both turbines, which is greater for a SW direction.

1. Introduction

The current energetic and environmental challenges induce a significant growth of the use of renewable energies. Wind energy production is undergoing intense research and development work. Conventional exploitation of this energy is carried out on a large scale in wind farms, whereas decentralised wind energy production, for example in the built environment, constitutes a relevant option [1]. Urban wind energy development raises several research questions. Amongst them, the optimal placement of small wind turbines in the vicinity of a building is still open.

Indeed, wind energy production is significantly affected by the upstream flow features. In urban areas, the presence of buildings causes complex turbulent phenomena [2] such as streamwise vortices, sweep events and other coherent flow structures, which occur at the bottom of the boundary layer. The operation of wind turbines located in this area of the urban boundary layer could thus be influenced by these complex flow motions. In general, wind turbines located downstream of buildings will be impacted by the flow slowed by the building, with a high level of turbulent kinetic energy. This will result in significant power losses and high velocity fluctuation at the wind turbine position [2]. Also taking into account that the wind does not always keep the same direction in a built environment, the optimal location of small wind turbines in these

areas, and the choice of a turbine technology, remains a major concern. In this framework, high fidelity numerical simulation can help to better understand how wind turbines work in complex environments.

There are two main families of wind turbines: *Horizontal Axis Wind Turbines* (HAWTs) and *Vertical Axis Wind Turbines* (VAWTs). HAWTs consist of blades whose axis of rotation is parallel to the ground surface. Thanks to the aerodynamic lift, the rotating blades extract on a horizontal axis, energy from an incident headwind. HAWTs are the most widely used and have been the subject of intense research and development, making them generally more efficient. VAWTs, on the other hand, consist of blades whose axis of rotation is perpendicular to the ground surface. The blades for this type of wind turbine rotate either by the effect of lift alone, by the effect of drag alone, or by a combination of both effects [3]. The advent of wind engineering in the built environment has led to the development of VAWTs, which have interesting advantages over traditional HAWTs. Unlike HAWTs, which must face the incident wind for optimum performance, VAWTs are omnidirectional and can receive wind from any direction, so they do not need wind tracking devices such as the yaw mechanism/motors. VAWTs can also be easily integrated in buildings, thanks to a three-dimensional design [4, 5, 6].

Comparative studies of the performance of the two families of wind turbines (HAWT and VAWT) have been documented in [3, 5, 7, 8], and have almost all come to the conclusion that for a constant speed headwind the HAWT has the best performance, while for a turbulent wind regularly changing direction the efficiency of the VAWT improves considerably. From this point of view, VAWT seems to be a good choice for installation in slower and more turbulent wind environments such as urban or industrial areas.

From another point of view, these studies were limited to comparing the performance of these two families of wind turbines, placed in empty environments, where the wind behavior is perfectly controlled from the inlet of the computational domain (or wind tunnel). There is only scarce literature on real urban environment investigations. The present work focuses on comparing the aerodynamic performance of a VAWT and a HAWT sized to produce the same electrical power over a realistic speed range. Both turbines are located close to a full-scale industrial building and are subjected to the same wind conditions. Two wind directions are investigated in this work to compare the wind turbines global behavior. Cases without building are also presented.

2. Methodology

2.1. Numerical model

In this study, Wall Modeled Large Eddy Simulations (WMLES) of HAWT and VAWT located close to a low-rise building will be performed. The governing fluid dynamics equations are the Navier-Stokes equations for incompressible flows, supplemented by a subgridscale (SGS) model,

$$\nabla \cdot \tilde{\mathbf{u}} = 0 \tag{1}$$

$$\frac{\partial \widetilde{\mathbf{u}}}{\partial t} + (\tilde{\mathbf{u}} \cdot \nabla)\tilde{\mathbf{u}} = -\nabla \widetilde{P} + \nu \nabla^2 \tilde{\mathbf{u}} + \nabla \cdot \tilde{\boldsymbol{\tau}}^M + \mathbf{f}\,. \tag{2}$$

The truncation operator, which consists in projecting a field on the LES grid, is written as $\widetilde{\bullet}$, $\widetilde{P} = \frac{1}{\rho}\widetilde{p}$ is the reduced pressure field, ν is the kinematic viscosity, and $\widetilde{\boldsymbol{\tau}}^M$ is the modeled SGS stress tensor. The body force $\mathbf{f}$ is introduced to model the effect of the wind turbine rotor onto the flow. The wind turbines blades considered here are modeled using an actuator line method [10, 12]. The LES equations are solved using the massively-parallel finite-volume solver YALES2 [9]. YALES2 features a central fourth order scheme on cartesian grid and uses a 4th-order Runge-Kutta time stepping. The code solves the incompressible Navier Stokes equations for turbulent flows on unstructured grids using a projection method for pressure-velocity coupling.

2.2. Turbulent inflow generation

The turbulence modeling at the inlet of the LES domain have a significant impact on the flow dynamics. In most cases, the generation of correct turbulent inflow conditions remains challenging. For the particular case of atmospheric boundary layer flow simulations, several methods for generating turbulent inflow conditions have been studied and compared [11, 13, 14, 15, 16]. Two of them are commonly used: synthetic methods and precursor methods. The basic idea for the synthesised turbulence methods is to construct a random field at the inlet of the domain that has appropriate turbulence characteristics (turbulence intensity and integral lengthscale). The precursor methods, on the other hand, consist of performing an auxiliary simulation of the wind flow on an independent domain with the same wall boundary conditions, in order to generate turbulence databases, which will be further used as an input condition for the main simulation. This realization of the flow can be computed before or in concurrency with the main simulation [11, 13]. Although compared to the synthesised turbulence methods they are more difficult to implement, and the total computational cost is higher due to the cost associated with this auxiliary simulation, this approach is more accurate [14, 16], as the turbulent conditions of the inflow are directly derived from Navier-Stokes dynamics and therefore contain realistic turbulent structures. In this work, the turbulent inflow will be generated by the precursor approach. In our case, the precursor will simulate a half-channel flow of height H, driven using a constant pressure gradient forcing (Eq. 3) , where u_τ is the wall friction velocity.

$$\left(\frac{dP}{dx}\right)_f = \frac{u_\tau^2}{H}\,. \tag{3}$$

Periodic boundary conditions imposed in the horizontal directions allow a relatively rapid generation of turbulent structures by recycling [11]. The flow thus reaches statistically stable conditions after a number of flow-through times.

3. Simulation framework

3.1. Building and wind conditions

The building used here is a real case of a low-rise building ($H = 8\,\mathrm{m}$) located in a typical industrial area (see Fig. 1 left) in Belgium. The site is characterised by a high turbulence intensity and roughness due to the environment. In the southern and northwestern sectors there are industrial buildings, houses and trees, while the northern and northeastern sectors do not contain any significant obstacles. Wind measurements were carried out on this industrial area in order to get an approximate value of the turbulence intensity. Through an anemometer placed 20 m above the building, velocity values were recorded every second for 6 months (from March to September 2021). They were then grouped by packets of 600 s (10 min) on which the calculations were carried out. Eq. 4 was used to determine the turbulence intensity, and at the end of the calculation, an approximate value of $TI \approx 17\%$ was retained:

$$TI[\%] = \frac{\sqrt{\langle u'^2 \rangle}}{\langle u \rangle} \times 100\,. \tag{4}$$

The most probable wind roses at the site are obtained using the numerical weather forecast model Aladin [17, 18, 19]. Four wind roses (see Fig. 1 right), each with 48 directions, were made based on available wind data from four years (2013, 2014, 2015, 2016). In 2013, the dominant wind direction was from the southwest (SW). In 2014, the prevailing wind shifted slightly to the south (S 1/6 SW). In 2015 it was rather south-southwest (SSW). In 2016 it was (SW 1/6 W). As for the north-east winds (NE), they are relatively weak compared to those from the south-west (SW) but cannot be neglected (2013). Four relevant wind directions can therefore be analysed :

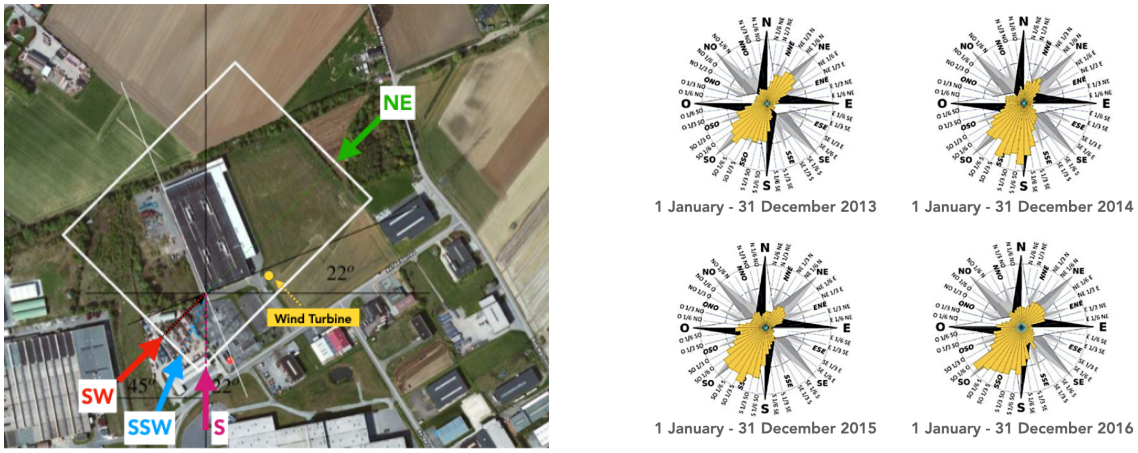

Figure 1: The building and its environment (left), and wind roses giving the dominant wind directions for this location (right).

SW, SSW, S and NE (see Fig. 1 left). In this work, the two most probable wind directions will be analysed first (SW and SSW).

3.2. Wind turbine parameters

This work compares two wind turbines designed to produce the same electrical power for a given wind speed: $u_{ref} = 5\,\mathrm{m/s}$. Figure 2 (left) shows the power curves of the two wind turbines. It is clear that for speeds between 3 and 8 m/s the two turbines are comparable, the two curves overlapping perfectly. The VAWT in this work is a 3-bladed straight wind turbine, consisting of a generic NACA profile for which the chord is $c_{Vawt} = 0.45\,\mathrm{m}$, similar to that currently installed on the site. The HAWT is a model derived from the NREL5MW, resized to produce the same power as the VAWT for the considered wind speed. Both turbines are evaluated on their optimum Tip Speed Ratio ($TSR = \omega r/u_{ref}$): $TSR_{\mathrm{Hawt}} = 7.55$ and $TSR_{\mathrm{Vawt}} = 3.65$, which result in a higher rotational speed for HAWT. The rotor of both wind turbines is located 20 m above the ground (see Fig.2 right).

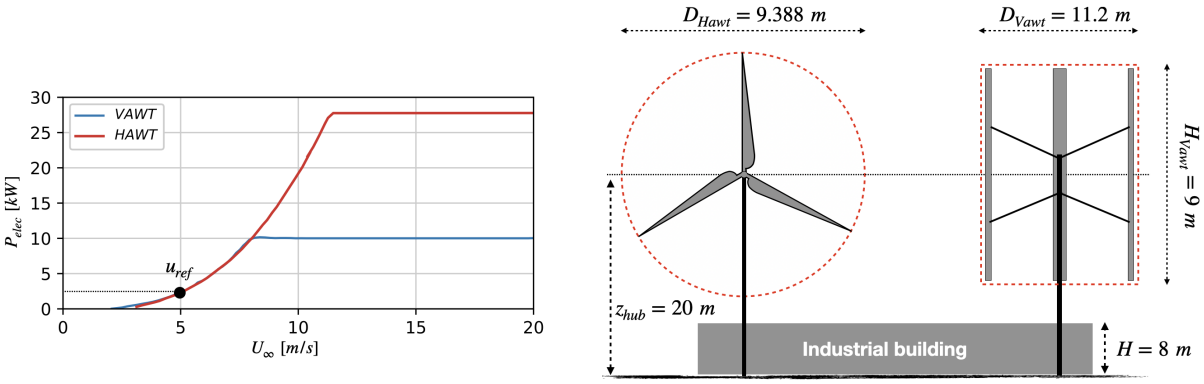

Figure 2: Power curves (left) and sizes (right) of the two wind turbines.

3.3. Numerical setup

The computational domain size is $1200 \times 1000 \times 150\,\mathrm{m}^3$, and the building is approximately 180 m long, 100 m wide and 8 m high (low-rise building). Its longest face is at an angle of 22° to the north direction and the mast of the wind turbine is located approximatly 17 m behind the building, with the rotor located 12 m above the building (see Fig. 3 left). The mesh, made using Gmsh software [20], is refined in the vicinity of the building, on the ground (see Fig.3 right) and in the wind turbine's wake up to 5 diameters after the rotor.

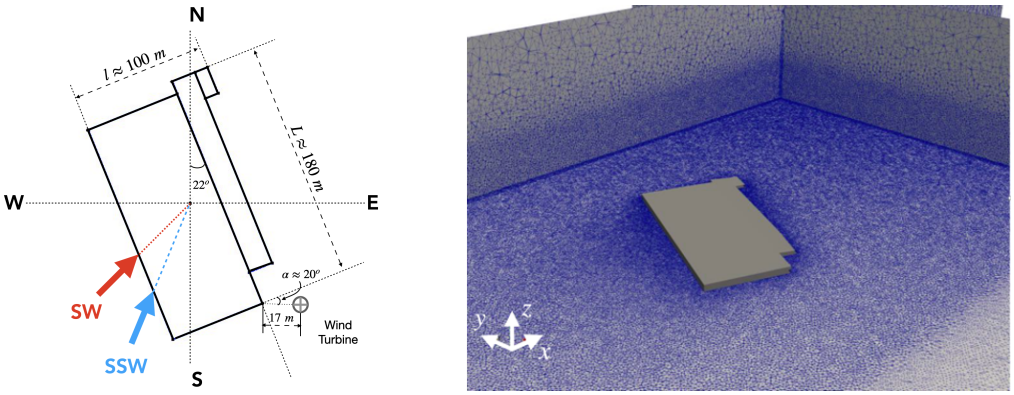

Figure 3: Building size and orientation (left), mesh of the computational domain for a SW wind direction (right).

The mesh resolution in the vicinity of the rotor was set to have 32 points per blade height for the VAWT and per radius for the HAWT. As the blade height of the VAWT is greater than the radius of the HAWT, its wake will be slightly coarser. The total mesh size includes $97M$ tetrahedral elements for VAWT cases and $100M$ for HAWT cases. For all simulations, the HAWT will be assumed facing to the incident wind, no dynamic stall model will be considered for the VAWT and the effect of the arms will be neglected. The σ-model will be used as a subgridscale (SGS) model [21].

A turbulent flow, obtained from the precursor simulation, is imposed at the inflow boundary. A convective boundary condition is applied at the outflow, slip wall boundary conditions in the transverse direction and at the top. At the bottom (the floor and walls of the building), a wall stress model for a rough wall is applied in order to compute the surface shear stress as a function of the LES velocity field at the first vertical grid point.

The precursor has the same cross-section as the inlet boundary of the computational domain, but is twice the domain in the streamwise direction. It simulates a velocity profile similar to that in Eq. 5, where the roughness length is here taken as $z_0 = 0.06\,\mathrm{m}$ (corresponding to an industrial area), and $\kappa = 0.37$. u_τ is determined so that $u_{ref} = 5\,\mathrm{m/s}$ at $z_{ref} = 20\,\mathrm{m}$. The streamwise average velocity profile obtained from the precursor simulation shows good agreement with the logarithmic law (see Fig.4 left):

$$u(z) = \frac{u_\tau}{\kappa}\, log\left(\frac{z + z_0}{z_0}\right) . \tag{5}$$

The TI level at the wind turbine hub is also in good agreement with the measured value at the site (see Fig.4 right).

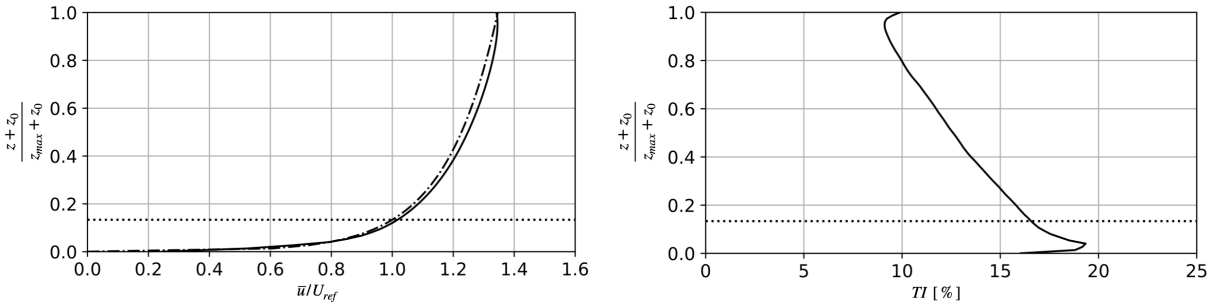

Figure 4: Left: comparison between the logarithmic law (-·-·-) and the vertical streamwise velocity profile obtained from the precursor (——). Right : Evolution of the TKE along the vertical direction in the precursor domain. The hub height of the wind turbines is also shown (·····).

4. Results

The different simulation cases carried out in this work are summarized in Tab. 1. $V0$ and $H0$ are respectively the VAWT and HAWT cases under the same wind conditions as the industrial site, but simulated without the low-rise industrial building. $V1$ and $H1$ are the respective simulations of both wind turbines with the low-rise industrial building, for a SW wind direction. $V2$ and $H2$ are similar to $H1$ and $V1$ but for a SSW wind direction. For each simulation case, a spin-up time corresponding to 6 crossings of the computational domain and a statistical accumulation time corresponding to 4 crossings of the computational domain were considered.

Table 1: Simulation cases.

Cases (color)	Wind Turbine	Building	Wind direction	Incident angle [°]
$V0$ (- - -)	VAWT	No	-	-
$V1$ (- - -)		Yes	SW	45
$V2$ (- - -)		Yes	SSW	67.5
$H0$ (——)	HAWT	No	-	-
$H1$ (——)		Yes	SW	45
$H2$ (——)		Yes	SSW	67.5

Figure 5 shows the turbulence intensity (TI) horizontal profiles at several downstream locations of the rotor of both wind turbines, for $V0$ and $H0$ cases. The profiles are taken at hub height. At $x/D = 0$, the TI of the incident wind is between 15 and 20% ($\approx 17\%$ at the rotor center point) for both wind turbines, which corresponds to that measured on the site. The wind conditions at the site are therefore well calibrated. From $x/D = 1$ to 2, the turbulence level in the rotor region is lower in the case of VAWT, before reaching that of HAWT from $x/D = 3$. The fact that the HAWT's near-wake turbulence level is higher than that of the VAWT may be due to the difference in the wake mesh resolution, finer for the HAWT case. However, it is interesting to see that the turbulence levels reach similar levels quite quickly in the far wake.

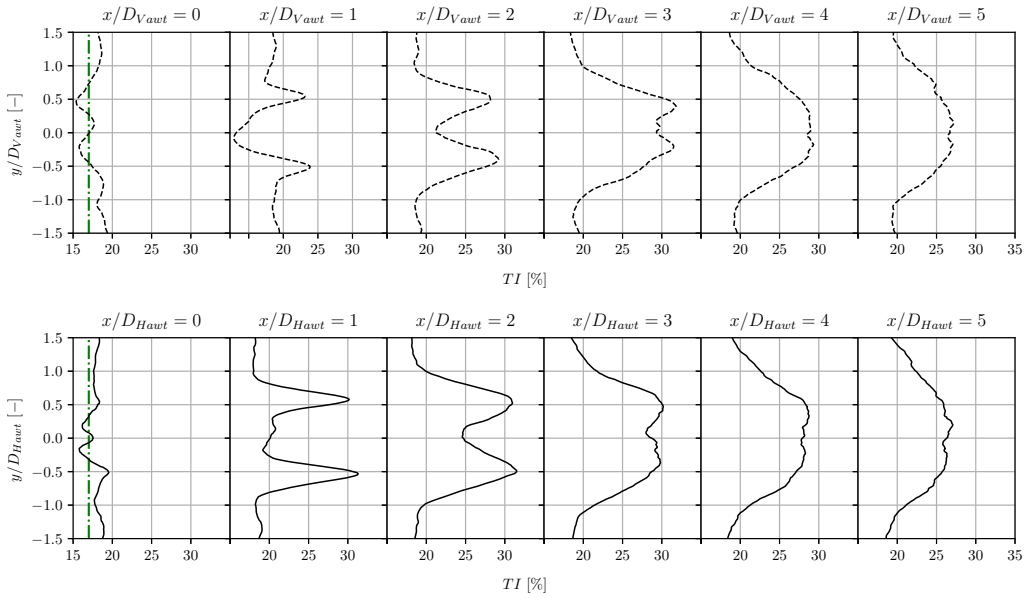

Figure 5: Horizontal profiles of TI profiles at several downstream locations of the rotor of the VAWT (top) and the HAWT (bottom). The measured experimental value is also indicated (-·-·-).

The building and wind direction effects on the wind turbines wake can be highlighted by analysing the results of the average wind speed and the Turbulent Kinetic Energy (TKE) produced by these wind turbines.

Figure 6 shows the time-averaged streamwise velocity in vertical slices for both VAWT and HAWT in the different simulation cases. The wakes are deflected to adapt to the inflow. This deflection is greater in the SW wind direction cases ($V1$ and $H1$), due to a local disturbance of the flow by the building, more pronounced in this case.

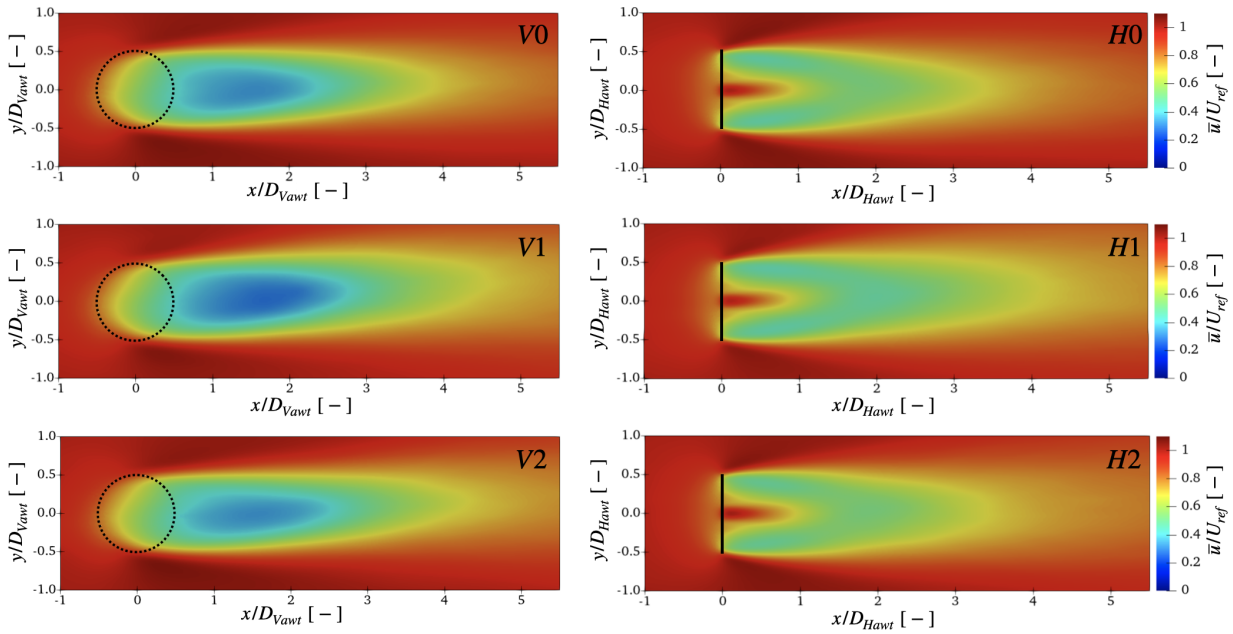

Figure 6: Horizontal slices of the time-averaged streamwise velocity for VAWT (left) and HAWT (right). $V0$ and $H0$ cases (top), $V1$ and $H1$ cases (middle), $V2$ and $H2$ cases (bottom).

In Fig. 7, the horizontal velocity profiles averaged in space and time show a local overspeed for both SW and SSW cases, up to $3D$ downstream of the rotor. This is due to the presence of the building which creates a local increase in flow velocity due to blockage. Due to the fact that it is a low-rise building compared to the hub height, these overspeeds are low: 4% and 2.4% for the SW ($V1$ and $H1$) and SSW ($V2$ and $H2$) cases respectively compared to the No-building case ($V0$ and $H0$).

A similar analysis can be made from the turbulent kinetic energy in the wake. Figure 8 presents vertical slices colored by the turbulent kinetic energy levels in the wake for the different simulation cases. The TKE levels depict a deflection in the wake following the flow direction. However, in the near wake, the TKE levels seem to be higher in the case of HAWT while in the far wake the trend seems to be reversed, the TKE levels produced by VAWT become higher. In order to confirm this result, the TKE profiles at several downstream locations of the rotor of the two wind turbines have been plotted in Fig. 9. The HAWT indeed features higher TKE levels in the near wake, perhaps still due to the difference in local wake resolution. For both wind turbines, the TKE levels are higher for the cases with a building ($V1$, $H1$, $V2$ and $H2$), and particularly for the SW wind case ($V1$ and $H1$).

In order to compare both VAWT and HAWT production, the power and thrust coefficients (C_P and C_T) have been calculated and averaged over time. The average values obtained are summarized in Tab. 2. Overall, the values of the HAWT are slightly higher, which was an expected result as most of the work in the literature came to the same result [3, 5, 7, 8].

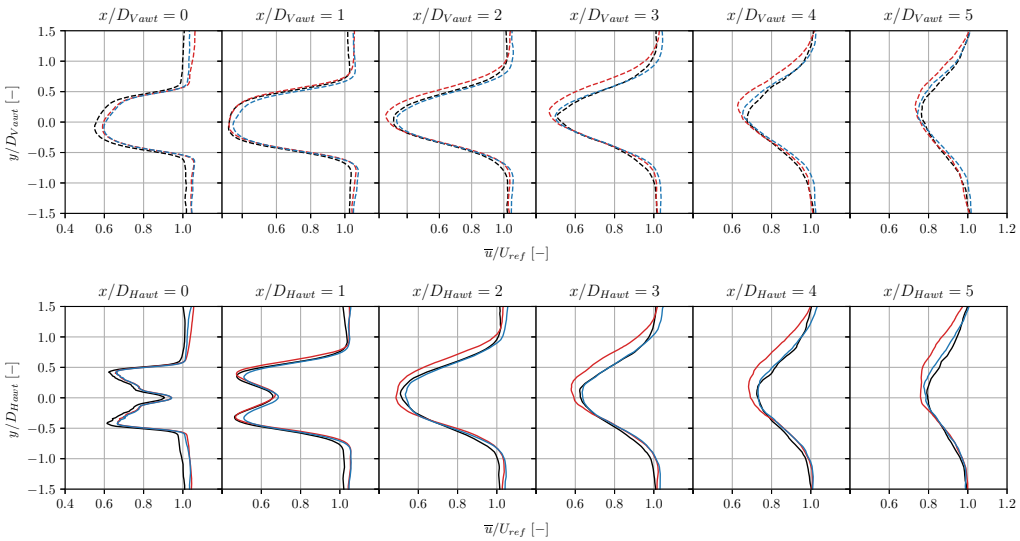

Figure 7: Horizontal profiles of the time-averaged streamwise velocity at several downstream locations of the rotor of the VAWT (top) and HAWT (bottom). $V0$ and $H0$ cases (—), $V1$ and $H1$ cases (—), and $V2$ and $H2$ cases (—).

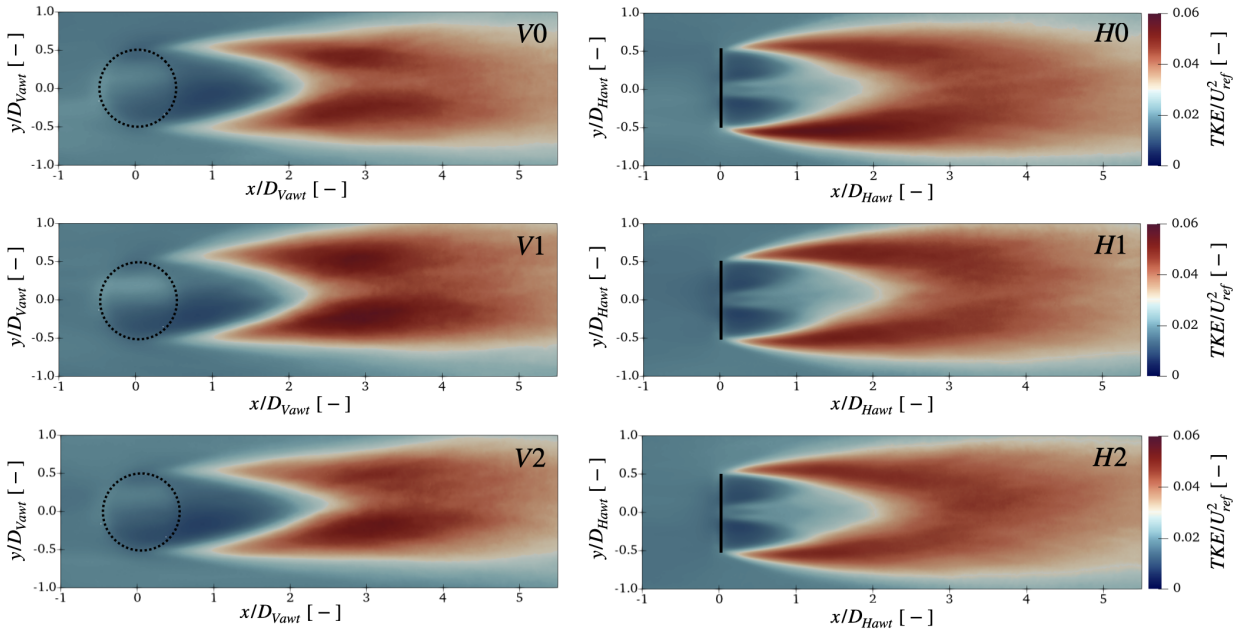

Figure 8: Horizontal slices of TKE for VAWT (left) and HAWT (right). $V0$ and $H0$ cases (top), $V1$ and $H1$ cases (middle), and $V2$ and $H2$ cases (bottom).

Furthermore, it is interesting to note that in the presence of the building, the $V1$ and $V2$ VAWT cases have an equivalent production to that of the $H0$ HAWT case, while it does not need additional devices to orient it towards the wind. It is also clear that, compared to the case without the building, the productions of both wind turbines are better in the presence of the building. Another interesting result would be that the VAWT productions are identical for both wind directions, whereas in the HAWT case the productions obtained for the SW direction ($H1$) is 2% higher than for SSW ($H2$).

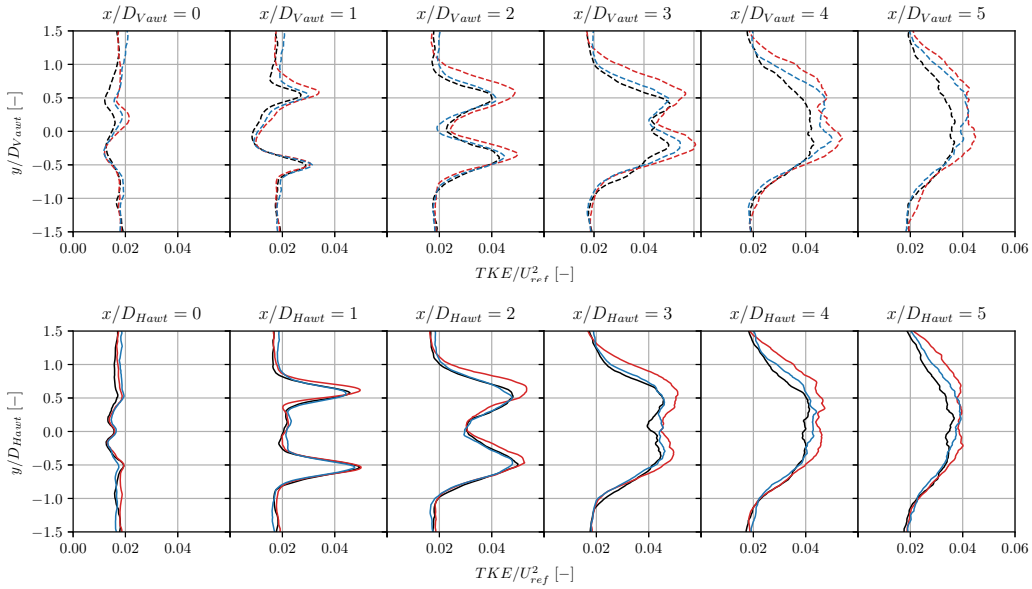

Figure 9: Horizontal profiles of TKE at several downstream locations of the rotor of the VAWT (top) and HAWT (bottom). $V0$ and $H0$ cases (—), $V1$ and $H1$ cases (—), and $V2$ and $H2$ cases (—).

Table 2: Power and Trust coefficients for VAWT and HAWT for the different simulation cases.

	$V0$	$H0$	$V1$	$H1$	$V2$	$H2$
C_P	0.4	0.42	0.42	0.46	0.42	0.45
C_T	0.72	0.71	0.75	0.75	0.75	0.74

5. Conclusion and future work

This study compares the aerodynamic performance of a VAWT and a HAWT located in the vicinity of a real low-rise industrial building, using WMLES coupled with an actuator line method. The methodology proposed here allows modelling the flows considered in a realistic way using state-of-the-art tools for the inflow turbulence, the wind turbines, and the building in a unified framework. The wind turbines are subjected to the same velocity and turbulence level, representative of field measurements. Both turbines are operating at their optimum TSR. First simulations, without the industrial building, showed that the turbulence intensity levels at hub height are close to the field measurements made at the industrial site. In a second time, the industrial building was introduced in the domain and two wind directions (SW and SSW) were investigated. The results, in this case, showed an overspeed up to $3D$ downstream of the rotor, amounting to 4% of the reference velocity. This overspeed remains quite low due to the fact that it is a low-rise building. The aerodynamic performance comparison (C_P and C_T) showed an overall better result for the HAWT, and an improvement in both wind turbines production in the presence of a building. The change of wind direction only slightly affects the performance of the HAWT while it has no influence on the VAWT. Although the two wind turbines compared here are specific models, a study based on two wind turbines of different models would lead to the same conclusions, provided that they are sized to produce the same power at a given wind speed, and that they are evaluated under the same wind conditions as proposed in this work. However, the selection between HAWT and VAWT would require further investigations. Indeed, due to the wind turbine proximity to a building an interest should be given to the noise levels. Since the turbulence levels considered are quite high, it could be also interesting to consider fatigue effects.

6. Acknowledgments

This research benefited from computational resources made available on the Tier-1 supercomputer of the Fédération Wallonie-Bruxelles, infrastructure funded by the Walloon Region under the grant agreement *No.* 1117545. Computational resources were also provided by the Consortium des Équipements de Calcul Intensif, funded by the Fonds de la Recherche Scientifique de Belgique under Grant No. 2.5020.11 and by the Walloon Region. Part of this work was funded by Walloon region under pole mecatech convention POPE C7961.

References

[1] Mertens S 2002 Wind energy in urban areas: Concentrator effects for wind turbines close to buildings *Refocus* **3** 22-24.
[2] Ge M, Gayme D F and Meneveau C 2021 Large-eddy simulation of wind turbines immersed in the wake of a cube-shaped building *Ren. En.* **163** 1063-77.
[3] Johari M K, A Jalil M A and Shariff M F M 2018 Comparison of horizontal axis wind turbine (HAWT) and vertical axis wind turbine (VAWT) *International Journal of Engineering & Technology* **7** (4.13) 74-80.
[4] Battisti L, Benini E, Brighenti A, Dell'Anna S and Raciti Castelli M 2018 Small wind turbine effectiveness in the urban environment *Ren. En.* **129** 102-13.
[5] Mendoza V, Chaudhari A and Goude A 2018 Performance and wake comparizon of horizontal and vertical axis wind turbine under varying surface roughness conditions *Wind Energy* **22** 458-472.
[6] Das A, Chimonyo K B, Kumar T R, Gourishankar S and Rani C 2017 Vertical axis and horizontal axis wind turbine- A comprehensive review*International Conference on Energy, Communication, Data Analytics and Soft Computing (ICECDS)* 2660-2669.
[7] Saad M. and Asmuin N 2014 Comparison of Horizontal Axis Wind Turbines and Vertical Axis Wind Turbines *Journal of Engineering* **04** 27-30.
[8] Fadil J, Soedibyo and Ashari M, 2017 Performance comparison of vertical axis and horizontal axis wind turbines to get optimum power output *15th International Conference on Quality in Research (QiR) : International Symposium on Electrical and Computer Engineering* 429-433.
[9] Moureau V, Domingo P and Vervisch L 2011 Design of a massively parallel CFD code for complex geometries *C.R. Mec.* **339** 141-48.
[10] Benard P, Viré A, Moureau V, Lartigue G, Beaudet L, Deglaire P and Bricteux L 2018 Large-Eddy Simulation of wind turbines wakes including geometrical effects *Computers and Fluids* **173** 133-39.
[11] Moens M 2018 *Large eddy simulation of wind farm flows: improved Actuator Disk model and investigations of wake phenomena* (Louvain: Ecole Polytechnique de Louvain) p 217.
[12] Sorensen J N and Shen W Z 2002 Numerical Modeling of Wind Turbine Wakes *Journal of fluids Engineering* **124** 393-99.
[13] Li Y, Cheng C, Lo Y, Fang F and Zheng 2015 Simulation of turbulentflows around a prism in suburban terraininflow based on randomflow generation method simulation *J. Wind Eng. Ind. Aerodyn.* **146** 51-58.
[14] Vasaturo R, Kalkman I, Blocken B and van Wesemael c 2018 Large eddy simulation of the neutral atmospheric boundary layer: performance evaluation of three inflow methods for terrains with different roughness *J. Wind Eng. Ind. Aerodyn.* **173** 241–61.
[15] Keating A, Piomelli U, Balaras E and Kaltenbach H 2004 A priori and a posteriori tests of inflow conditions for large-eddy simulation *Phys. Fluids* **16**(12) 4696–4712.
[16] Tabor G R and Baba-Ahmadi M H, 2010 Inlet conditions for large eddy simulation: A review *Computers & Fluids* **39** 553–567.
[17] Farda A, Déqué M, Somot S, Horányi A, Spiridonov V and Tóth H 2010 Model ALADIN as Regional Climate Model for Central and Eastern Europe *Stud. Geophys. Geod.* **54** 313-332.
[18] Žagar N, Žagar M, Cedilnik J, Gregorič G and Rakovec J 2006 Validation of mesoscale low-level winds obtained by dynamical downscaling of ERA40 over complex terrain *Tellus* **58A** 445–455.
[19] Hrastinski M, Horvath K, Plenković I O, Ivatek-Šahdan S and Bajić A 2015 Verification of the operational 10 m wind forecast obtained with the ALADIN mesoscale numerical weather prediction model *Croatian Meteorological Journal* **50** 105-120.
[20] Geuzaine C and Remacle J-F 2009 Gmsh: a three-dimensional finite element mesh generator with built-in pre- and post-processing facilities. *International Journal for Numerical Methods in Engineering* **79**(11) 1309-31.
[21] Nicoud F, Toda B H, Cabrit O, Bose S and Lee J 2011 Using singular values to build a subgrid-scale model for large eddy simulations *Phys. Fluids* **23**(8) 085106.